

Article

Comparison of Geometrical Layouts for a Multi-Box Aerosol Model from a Single-Chamber Dispersion Study

Alexander C. Ø. Jensen ^{1,*} , Miikka Dal Maso ², Antti J. Koivisto ¹ , Emmanuel Belut ³ , Asmus Meyer-Plath ⁴ , Martie Van Tongeren ⁵, Araceli Sánchez Jiménez ⁶ , Ilse Tuijnman ⁷, Maida Domat ⁸, Jørn Toftum ⁹  and Ismo K. Koponen ¹⁰

¹ The National Research Centre for the Working Environment, Lersø Parkallé 105, 2100 Copenhagen, Denmark; jok@nrcwe.dk

² Aerosol Physics, Laboratory of Physics, Faculty of Natural Sciences, Tampere University of Technology, Korkeakoulunkatu 10, FI-33720 Tampere, Finland; miikka.dalmaso@tut.fi

³ Institut National de Recherche et de Sécurité (INRS), Rue du Morvan CS 60027, 54519 Vandoeuvre CEDEX, France; emmanuel.belut@inrs.fr

⁴ Bundesanstalt für Arbeitsschutz und Arbeitsmedizin, Nöldnerstr. 40-42, 10317 Berlin, Germany; meyer-plath.asmus@baua.bund.de

⁵ Centre for Occupational and Environmental Health, The University of Manchester, Oxford Rd., Manchester M13 9PL, UK; Martie.J.Van-Tongeren@manchester.ac.uk

⁶ Institute of Occupational Medicine, Research Ave N, Currie EH14 4AP, UK; Araceli.Sanchez@iom-world.org

⁷ TNO, Lange Kleiweg 137, 2288 GJ Rijswijk, The Netherlands; ilse2271969@gmail.com

⁸ Instituto Tecnológico del Embalaje Transporte y LOGÍSTICA, C/ Albert Einstein, 1, 46980 Paterna, Spain; maida.domat@itene.com

⁹ Department of Civil Engineering, Technical University of Denmark, Anker Engelunds Vej 1 Bygning 101A, 2800 Kongens Lyngby, Denmark; jt@byg.dtu.dk

¹⁰ Force Technology, Park Allé 345, 2605 Brøndbyvester, Denmark; ik@force.dk

* Correspondence: alj@nrcwe.dk; Tel.: +45-3916-5201

Received: 19 February 2018; Accepted: 22 April 2018; Published: 24 April 2018



Abstract: Models are increasingly used to estimate and pre-emptively calculate the occupational exposure of airborne released particulate matter. Typical two-box models assume instant and fully mixed air volumes, which can potentially cause issues in cases with fast processes, slow air mixing, and/or large volumes. In this study, we present an aerosol dispersion model and validate it by comparing the modelled concentrations with concentrations measured during chamber experiments. We investigated whether a better estimation of concentrations was possible by using different geometrical layouts rather than a typical two-box layout. A one-box, two-box, and two three-box layouts were used. The one box model was found to underestimate the concentrations close to the source, while overestimating the concentrations in the far field. The two-box model layout performed well based on comparisons from the chamber study in systems with a steady source concentration for both slow and fast mixing. The three-box layout was found to better estimate the concentrations and the timing of the peaks for fluctuating concentrations than the one-box or two-box layouts under relatively slow mixing conditions. This finding suggests that industry-relevant scaled volumes should be tested in practice to gain more knowledge about when to use the two-box or the three-box layout schemes for multi-box models.

Keywords: aerosol modelling; dispersion factor; geometry; chamber study; multiple boxes; occupational exposure

1. Introduction

As the production and use of nanomaterials increases [1–4], workers are increasingly being exposed to aerosol nanoparticles that were released during the production or reworking [5], with potential adverse health effects [6]. Pre-emptive assessment of exposure using mathematical mass balance models can aid the workplaces in implementing risk management measures for working in environments handling nanoparticles.

Chamber measurements are essential for testing and validating the dispersion models used for exposure assessment. Dispersion of both gases and particles in chambers has previously been studied with included relevant aerosol dynamics and chemistry [7]. Several approaches and implementations of computational exposure exist; examples include single-box, multi-box, and multi-compartment models (see, e.g., Johnson et al. [8], Zhang et al. [9], and Nazaroff [10]), Eulerian models [11], Gaussian plume models [12,13], Lagrangian models [14,15], and Markov's chain models [16]. The most widely used model for indoor environments is the well-established box model [17]. The box model assumes a well-mixed chamber where the concentrations are instantly mixed in the entire volume. However, this is not always the case. Furtaw et al. [18] and Nicas et al. [19] studied SF₆ gas concentrations in an imperfectly mixed chamber and the concept of a near field (NF) zone with higher concentrations than the far field (FF) zone was introduced. The box model was further developed by Cherrie and Schneider [20], and has been expanded to include several individual compartments in which airflow is restricted by physical barriers, such as walls [10,21,22]. The ventilation of the well-mixed two-box model was studied by Cherrie et al. [23] and has further been analysed to include also various setups of local ventilation controls and recirculation by Ganser and Hewett [24], and has been used to model concentrations in workplaces by Koivisto et al. [25].

At the same time, a series of efforts to aid companies with assessing potential exposure to workers have been done by developing guidelines and control banding and exposure analysis tools. These tools include, e.g., ECETOC TRA [26], to evaluate exposure and risk using exposure scenarios, which can further be combined with probabilistic models, or conceptual near-field/far-field models that are based on the model by Cherrie et al. [20], such as Stoffenmanager [27] and the Advanced REACH Tool [28].

In real-world rooms, the air is rarely fully mixed. The processes might be fast and rapidly changing, or the ventilation system might be limited or not effective and other mixing factors, such as turbulence from movement or convection dominates the mixing, as seen for example in the study by Jensen et al. [29]. Thus, in some cases, there should be more than two compartments to allow for longer mixing times and better granularity of the concentration gradient. However, there are no chamber studies conducted to test multi-compartment models as the number of measured reference points has been too limited.

In the presented work, we monitored six different positions in an 80 m³ chamber using three fast mobility particle sizers (FMPS), a scanning mobility particle sizer (SMPS), and five condensation particle counters (CPC). We dispersed NaCl using a nebulizer system with a characterized source, to produce data for modelling studies using either a constant or pulsating source as input for an aerosol model that was based on the multi-box approach. Four different geometrical layouts in the multi-box model were used to compare modelled concentrations with the measured concentrations. The aim of our study was to explore the optimal way to model aerosol dispersion using a multi-compartment approach, and to determine whether the added complexity and the parameters that were introduced by the additional compartments present a significant benefit.

2. Materials and Methods

2.1. Description of the Model

The aerosol model that is presented here is based on existing and well-established aerosol dynamics particle population balance equations. The total particle population balance equation that

describes the change in number concentration per time is given by the simplified general dynamics equation (see, e.g., Seinfeld and Pandis [30]; Jacobson [31])

$$\frac{dN_{k,i}}{dt} = J_{\text{source},k,i} + J_{\text{exchange},k,i} + J_{\text{coagulation},k,i} + J_{\text{deposition},k,i} \quad (1)$$

where $\frac{dN_{k,i}}{dt}$ ($\text{m}^{-3} \text{s}^{-1}$) is the change in number concentration over time in box k and for size bin i in the size distribution is used to characterise the source. i can be defined from a measurement following the bin division in the instrument or for a source that is based on a lognormal distribution. k can assume values, such as b_{NF} , b_{FF1} , b_{FF2} , \dots , and b_{FFx} , depending on the chosen geometry. $J_{\text{source},k,i}$ is the particle generation term, defined only in the NF zone, i.e., if $k = \text{NF}$. $J_{\text{exchange},k,i}$ is the ventilation-induced transport term between the boxes. $J_{\text{coagulation},k,i}$ describes the contribution of coagulation occurring in the boxes. $J_{\text{deposition},k,i}$ is the removal of particles due to deposition.

2.1.1. Source

The source term describes the origin of pollutants in the system. The source position is at all times assumed to be a single point source that is contained in the centre of the NF volume and particles are released from the source into the NF. The source term can be written as

$$J_{\text{source},k,i} = 0 \text{ if } k \neq \text{NF} \text{ and } J_{\text{source},\text{NF},i} = \frac{S_i}{V_{\text{NF}}} \quad (2)$$

where S_i [s^{-1}] is the source strength either estimated from measurements or simulated using a fixed lognormal particle size distribution. V_{NF} (m^3) is the volume of the near field.

For a measured source, S_i is defined as

$$S_i = C_{\text{source measured},i} \times f_{\text{dispersion}} \times F_{\text{flow rate}} \quad (3)$$

where $C_{\text{source measured},i}$ [m^{-3}] is the concentration measured in the source position. $f_{\text{dispersion}}$ is the dispersion factor applied to the measured concentration as a fitting parameter. Effectively, the parameter $f_{\text{dispersion}}$ describes the underestimation of the source concentration by taking into account the dispersion that is occurring between the source point and the measurement position. If the $C_{\text{source measured},i}$ is measured inside the source outlet the $f_{\text{dispersion}} = 1$. If the $C_{\text{source measured},i}$ is measured nearby the source and not inside the source outlet the concentrations need to be scaled according to the immediate dispersion and dilution occurring between the outlet and the measurement point. $F_{\text{flow rate}}$ [$\text{m}^3 \text{s}^{-1}$] is the volumetric flow rate of the source, as measured at the source outlet.

2.1.2. Transport and Ventilation

It is assumed that each box is well-mixed and the general ventilation is the main driver for transport processes in the system. The transport $J_{\text{exchange},k,i}$ between box k and connected boxes for the size bin i (in $\text{m}^{-3} \text{s}^{-1}$) is given by Equation (4)

$$J_{\text{exchange},k,i} = \frac{1}{V_k} \sum_l (Q_{lk} N_{l,i} - Q_{kl} N_{k,i}) \quad (4)$$

where l is a different box in the chamber as defined by the geometry or the inlet and exhaust, V_k is the volume [m^3] of the box, N is the number concentration [m^{-3}] of particles, and Q_{kl} is the air flow rate [$\text{m}^3 \text{s}^{-1}$] from box k to box l , positive or zero, by definition. This equation also encompasses the introduction or the removal of particles from the system by the general room ventilation inlet and exhaust. In the case of the inlet and exhaust, the inflow concentration is in this work that is assumed to be 0 m^{-3} .

Equation (4) is necessarily completed by the conservation of air mass in each box k , which reads:

$$\sum_{l=1}^{n_{\text{boxes}}} Q_{lk} = \sum_{l=1}^{n_{\text{boxes}}} Q_{kl} \quad (5)$$

The flow rate Q between the boxes and to the exhaust is driven by the general room ventilation. While the air exchange rate (AER) into and out of the chamber can be measured accurately, the air flow rate between boxes Q_{kl} affecting the $J_{\text{exchange},k,i}$ parametrisation has to be estimated in most cases.

2.1.3. Coagulation

The description of coagulation is based on the modified Fuchs equations [32], which account for coagulation due to the Brownian diffusion; this is the most relevant process for submicron particles. The number concentration change rate [$\text{m}^{-3} \text{s}^{-1}$] from the process of coagulation is given by the term $J_{\text{coagulation},k,i}$

$$J_{\text{coagulation},k,i} = \frac{1}{2} \sum_{j=1}^{i-1} K_{j,i-j} N_{k,j} N_{k,i-j} - N_{k,i} \sum_{j=1}^{\infty} K_{i,j} N_{k,j} \quad (6)$$

where K [$\text{m}^3 \text{s}^{-1}$] is the Fuchs coagulation coefficient [32] between particles. Here, the contribution from the coagulation is the removal of particles from certain size bins and the addition of the combined particle to the appropriate combined size bin by keeping the total volume constant and by considering the diameter of the corresponding sphere of similar volume. In the case that two particles collide and end up in the largest size bin, the number concentration is adjusted accordingly for mass conservation.

2.1.4. Deposition

Deposition is the process of removal of aerosol particles that are adhering to surfaces in the chamber. In this model, the process is irreversible, since resuspension is not considered. The treatment of deposition is based on the equations that are presented in Lai and Nazaroff [33]. This way of calculating deposition velocities gives a general, size-dependent term for depositional losses. However, the developed model may be modified to use other deposition schemes. The time-dependent change in particle number concentration [$\text{m}^{-3} \text{s}^{-1}$] is given by

$$J_{\text{deposition},k,i} = - \frac{1}{V_k} \sum_r A_{k,r} v_{k,r,i} N_{k,i} \quad (7)$$

Here, A is the area [m^2] that is available for deposition in the direction r , which can be chosen as upwards, downwards, or vertical surfaces. v is the size-dependent deposition velocity [$\text{m} \text{s}^{-1}$]. To calculate the deposition velocity, the density and the friction velocity is needed. In this work, we assumed a constant density of 1 g cm^{-3} for all of the particles and a friction velocity of 0.01 cm s^{-1} , which is the same as estimated by Shi and Zhao [34] for normal indoor environment without fan mixing. The surface area that is available for deposition in each box changes according to the user defined geometrical layout.

2.1.5. Solving the General Dynamics Equation

The general dynamics equation was implemented as a MATLAB function and was solved using an ordinary differential equation (ODE) solver inherent in MATLAB [35]. The ODE solver is a numerical solver that calculates for each time step the changes in concentration in each size bin of the aerosol and each box in the volume, as defined by the user. The numerical ODE solver used was the non-stiff ODE45 solver, which uses a variable four step Runge-Kutta Dormand–Prince method [36] using single step solving with a relative tolerance between consecutive points of 10^{-6} . Sensitivity analysis of the model was done using a one-at-a-time analysis [37], as described in the Supplementary Material Figures S1–S4.

2.2. Experimental Work

The referenced experimental work was carried out at a chamber facility at the Technical University of Denmark. The dimensions of the chamber were ($h \times l \times w$) $2.65 \times 6.45 \times 4.72 \text{ m}^3$, with a total volume of 80.7 m^3 . The chamber was ventilated with HEPA filtered air. Volumetric flow into and out of the chamber was measured with a balometer (SwemaFlow 125, Swema, Stockholm, Sweden). The chamber was monitored at six measurement points that were evenly distributed in the chamber and at a height of 160 cm: near the source, NF, FF1, FF2, FF3, and FF4. Number concentrations of the aerosolised NaCl were measured in all points, while size distributions were measured in all of the points except FF1 and FF3. NaCl was aerosolised using a nebuliser (AGK 2000, Palas, Karlsruhe, Germany) in 0.1 w/w % concentration and was dispersed either as a constant source or as a series of pulses from a constant height of 120 cm. The aerosol instruments used, positions, and detailed descriptions hereof can be found in supplementary Table S5. The experimental set-up can be seen in Table 1. All of the concentrations were measured through conductive copper tubing of 2.6 m. Diffusion losses were corrected according to Cheng [12] when possible. For detailed information on the experimental work see the Nanoreg report D3.4 [38].

Table 1. Geometrical layouts used as input for the model with respective names for the modelled concentrations, positions of measurements, exhaust, and source location. Gridlines represents 1 m spacing. One-box layout G1, a two box layout G2, and two three-box layouts G3 and G3c. Volumes and areas available for deposition in various directions facing up, A_U , facing down, A_D , and with vertical facing, A_V .

		b_{NF}	b_{MF}	b_{FF}
<p>G1</p>	V [m^3]	80.7	-	-
	A_U [m^2]	30.4	-	-
	A_D [m^2]	30.4	-	-
	A_V [m^2]	59.2	-	-
<p>G2</p>	V [m^3]	8	-	72.7
	A_U [m^2]	0	-	30.4
	A_D [m^2]	0	-	30.4
	A_V [m^2]	0	-	59.2
<p>G3</p>	V [m^3]	8	45.8	26.9
	A_U [m^2]	0	20.3	10.1
	A_D [m^2]	0	20.3	10.1
	A_V [m^2]	0	35.3	23.9
<p>G3c</p>	V [m^3]	6.4	34.7	39.6
	A_U [m^2]	2.4	13.1	14.9
	A_D [m^2]	2.4	13.1	14.9
	A_V [m^2]	0	20.9	38.3

Two steady state experiments, E1 and E2, were chosen as providing a scenario with a constant source in high and low AER, respectively, and E3 with a rapidly changing pulsating source in low AER. These experiments were chosen since they have the most complete datasets for all instrument used. E1, E2, and, E3 corresponds to DTU04, DTU06, and DTU09, respectively, as found in the Nanoreg report D3.4. For E1 and E2, the SMPS data measured near the source during the experiments have been used as the input to the model as the source term. For E3, the SMPS neutralizer was not active during the experiments. The source input has therefore been constructed using the product of the normalised total number concentrations from experiment E3 and the mean size distribution that was measured during the steady state period of E2.

2.3. Description of Geometries Considered

The main focus here is to compare a one-, two-, or three-box geometrical layout, and to investigate whether there is a need to add additional boxes to the systems. This concern is important, as adding a more complex geometry increases the number of free variables, the computational time, and the uncertainty of the user-required input. However, if the ability to predict the concentrations improves, it may be worth the effort. Four different geometrical setups (Table 1) were chosen to represent different ways to divide the chamber. A one-box layout (G1) where the entire chamber was considered as a single box. A two-box layout (G2) with a NF volume of 2^3 m^3 and the FF was the rest of the chamber. In one of the two considered three-box layouts (G3), the NF was the same as for the two-box layout, but the rest of the chamber was divided into a mid field (MF) and a FF two along the longest wall at $2/3$ of the length. In the other three-box layout (G3c), the chamber was divided into a series of concentric cylinders with full chamber height with the source at the centre. The diameter of the NF is 1.75 m, the radius of the MF was 3 m, and the FF was the rest of the chamber. The diameter of the NF was chosen according to the geometry. The NF measurement position was 0.71 m from the source. The radius of the NF in G3c was then chosen to contain the NF measurement point. The volumes and areas available for deposition for each layout can be found in Table 1.

Mixing and Transport

The only driving system for ventilation, transport, and mixing in the chamber was the supply and the extraction of air to the chamber positioned in in the ceiling of the chamber. The supply air was filtered by HEPA H14 filters and inlets were fitted with a diffuser for an even spread of the incoming clean air. Any mixing due to convective flows was assumed to be insignificant when compared with the mixing due to the ventilation. For $J_{\text{exchange},k,i}$, the flow rate between connected boxes, were calculated from the AER of the room.

$$Q_{kl} = Q_{lk} = \text{AER} \times V_{\text{total}} \times \frac{1 \text{ h}}{3600 \text{ s}} \quad (8)$$

Q_{kl} was naturally set to zero when boxes k and l were not connected. Any flow out from leaks or instruments, as well as, flow in from the source nebuliser was neglected. The exhaust removal process is set to occur in the conceptual box where the outlet is located (Table 1). This method of calculating the flow rates is useful for well-mixed volumes, while in other ventilation settings, the flow might need to be calibrated as done, e.g., in Ganser and Hewett [24]. In this study, for the AER of 3.5 h^{-1} and 10 h^{-1} Q between connected boxes was $0.0785 \text{ m}^3 \text{ s}^{-1}$ and $0.2242 \text{ m}^3 \text{ s}^{-1}$, respectively.

3. Results

3.1. Particle Concentration Measurements

The nebuliser provided a stable concentration and size distribution of NaCl aerosols, as measured above the source. The generated particles have a geometric mean diameter of 42 nm and turning off the nebuliser caused the concentrations to rapidly decrease (Figure S6). Particle number concentrations

in the chamber were measured during the experiments with a time resolution of 1 s but were averaged to a time resolution of 60 s to improve readability, Figure 1. In general, the measured concentrations agreed well within each measurement position with CPC total number concentrations being 0.7 times the corresponding FMPS concentrations; this is due to the lower cut off size in the FMPS and the multi charging on agglomerates, which causes some overestimation of the FMPS concentration [39]. Higher concentrations were measured by the CPCs in positions FF1 and FF3 when compared to positions FF2 and FF4, with FF2 concentrations being higher than FF4 concentrations. In the E1 and E2 experiments, the source was continuously on and the AER was 10 h^{-1} in E1 and 3.5 h^{-1} in E2. The NF concentrations during the time when the source was active were on average 4.5 and 1.5 times higher than the FF concentration, respectively (Figure 1A,B). When the source was turned off, the NF and FF concentrations were similar in both cases. At steady state, the results from the high AER experiment show separation into a well-mixed NF or FF zone, whereas for low AER concentrations were similar in the entire chamber. In the E3, the source emission was pulsed at cycle of 2 min on and 15 min off and the cycle was repeated seven times, and the AER was 3.5 h^{-1} (Figure 1C). For E3 the average concentration in the NF when the particles were released was 2.2 times higher, with peak concentrations up to 10 times higher than the average FF concentrations. There was a delay in time between peak concentrations at different positions with approximately 300 seconds delay between the NF peak concentration position and the peak concentration of FF4 furthest from the source. In some instances, the FF3 concentrations were higher than what was measured in the NF. Size distributions that were measured by the FMPS in NF, FF2, and FF4 positions are found in Figure S7.

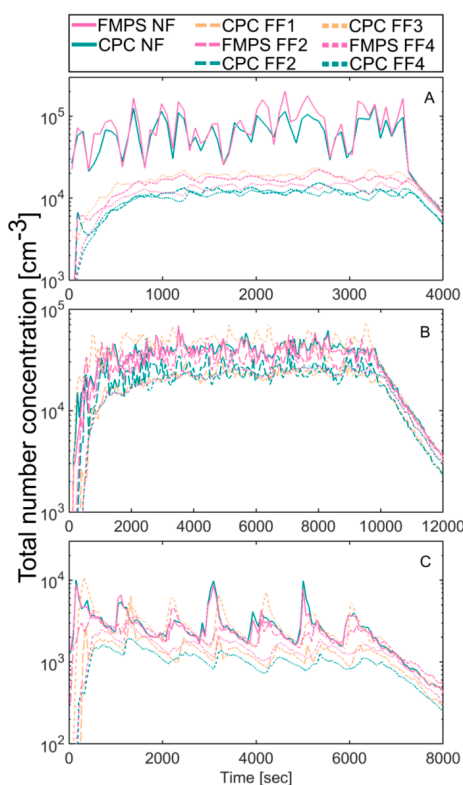


Figure 1. Measured aerosol total number concentrations in the chamber during experiment E1 (high air exchange rate (AER) and constant source) (A); E2 (low AER and constant source) (B); and, E3 (low AER and fluctuating source) (C).

3.2. Modelled Concentrations

The source measurement position was placed 40 cm above the outlet of the nebulizer, and a dispersion factor of 18 ± 0.1 provided the best fit in the case of fast mixing, E1, whereas 4.2 ± 0.1

was found as the best fit for both sources in the slow mixing system, E2 and E3. The best fit was determined by minimising the overall deviation between the measured and modelled the total number concentrations. Mass balance for the modelled two-box layout can be found in Figure S8.

As expected, when the number of compartments was increased the model predicted better local concentrations measured different locations of the room. In E1 the one-box layout, G1, underestimated the NF concentrations by 60%, while FF concentrations were mainly overestimated. For the two-box layout and the two three-box layouts, G2, G3, and G3c, respectively, the NF concentrations were underestimated by 25%, while FF concentrations were mainly overestimated. When comparing by position and instrument, the calculated deviations from the measured concentrations of two- and three-box layout, they were within ± 8 percentage points of each other (Figure 2). This meant that concentrations were estimated equally for the multi-box layouts.

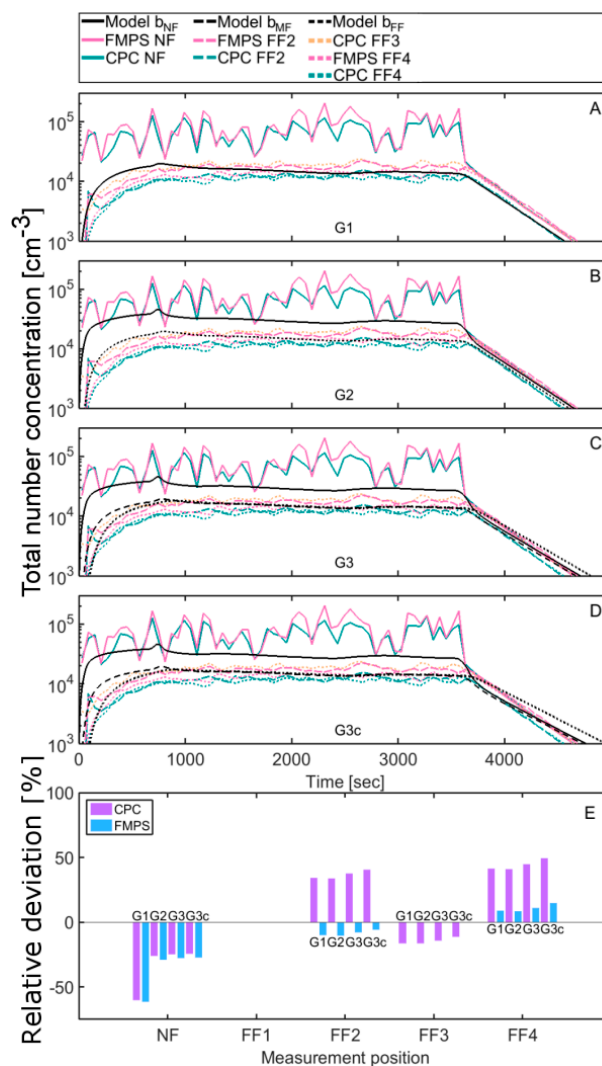


Figure 2. Results from the modelling of experiment E1. (A) shows the results from the one-box layout G1; (B) shows the results for the two-box layout G2; and, (C,D) are the results from the two three-box layouts G3 and G3c, respectively; (E) shows the geometric mean of the deviation that have been calculated between the measurement position and the box representing the position, e.g., b_{MF} in the case of the FF2 for the three-box layouts.

In E2, for the one-box layout, the NF concentrations were underestimated by 40%, while the two-box layout overestimated the NF concentrations by 12%. The concentrations in the FF positions

were predicted similarly by all of the layouts, and were ± 7 percentage points within each other, regardless of geometrical layout, when comparing by position and instrument the deviation from the modelled concentrations (Figure 3). For the two steady state experiments, E1 and E2, the differences between the two-box and the three-box layouts were mainly due to differences in the establishing phase of the steady state and at end of the experiment, after the source was turned off. During the steady state, the modelled concentrations were similar for all of the geometrical layouts. Additionally, the multi-box layouts estimated more accurately the NF concentrations, than the one-box layout. At the same time the modelled concentrations for the far field were similar between the two- and three-box layouts, but the complexity was lower for the two-box layout because of the simpler geometry. Therefore, for both E1 and E2 the two-box layout provided the optimal geometrical layout.

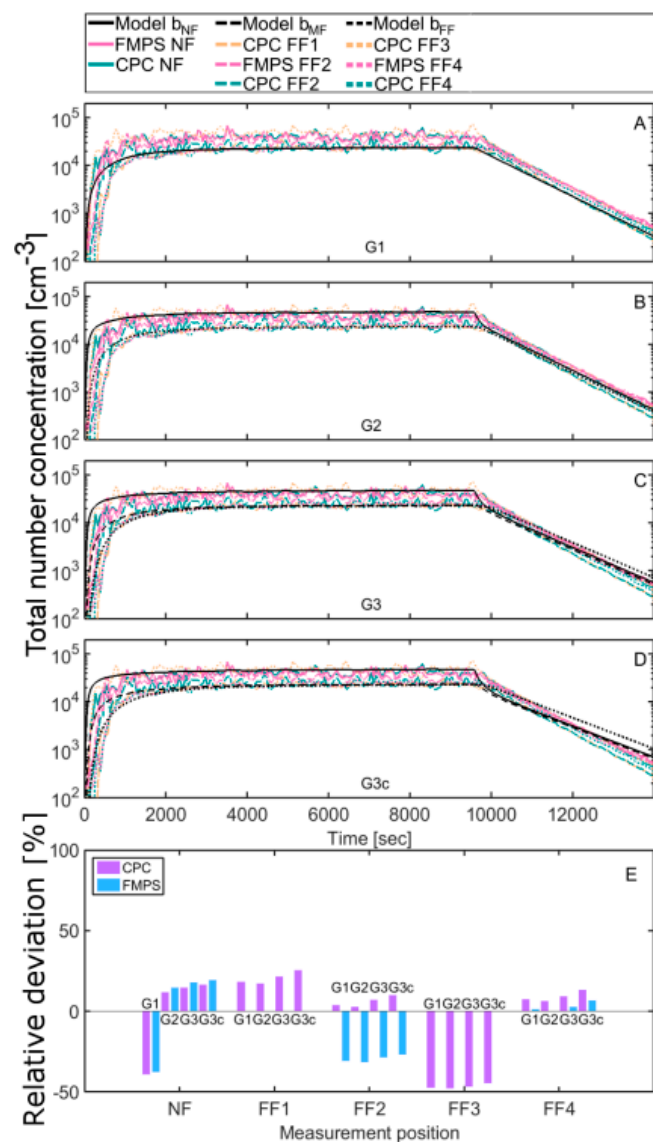


Figure 3. Results from the modelling of experiment E2. (A) shows the results from the one-box layout G1; (B) shows the results for the two-box layout G2; and, (C,D) are the results from the two three-box layouts G3 and G3c, respectively; and, (E) shows the geometric mean of the deviation that have been calculated between the measurement position and the box representing the position, e.g., b_{MF} in the case of both FF1 and FF2 for the three-box layouts.

In E3, the constructed source strength was found to generate concentrations in a similar order of magnitude as the measured concentrations. For the one-box layout the NF concentrations were underestimated by 40%. The NF concentrations were predicted within $\pm 10\%$ using the more complex geometrical layouts. The G3c provided the lowest deviation of $\pm 2\%$. For positions FF1 and FF4 the concentrations were overestimated by all geometrical layouts, while the three-box layouts provided the lowest deviations of the tested geometries with a deviation of 30% and 48% when comparing with the CPC, respectively, and 0% when comparing with the FMPS concentrations that were measured in FF4. For FF2 and FF3, the concentrations were underestimated by all layouts by 25–48% (Figure 4). In addition, the three-box layouts successfully estimated the broadening of the concentration profile and the timing of the peak concentrations within $\pm 2\%$ for the FF1 and FF4 measurement positions as compared with the one- and two-box layouts, and less than 5% difference in timing for the FF2 position (Figure S9). Comparing the measured and the modelled particle size distributions showed that the model was able to replicate well the size distribution profiles, which followed the same overall shape between the experiments and the modelled distributions (Figure S7).

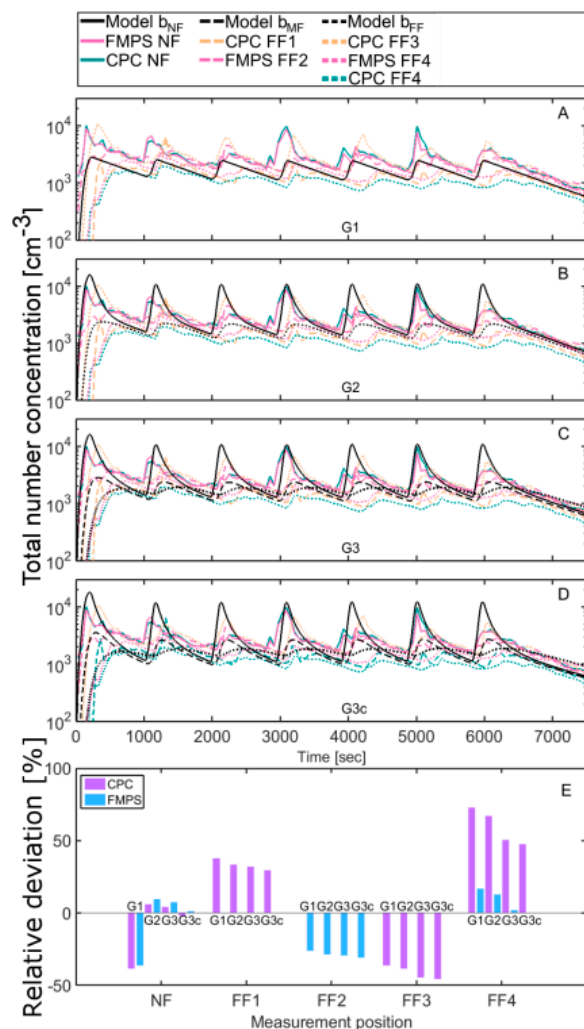


Figure 4. Results from the modelling of experiment E3. (A) shows the results from the one-box layout G1; (B) shows the results for the two-box layout G2; and, (C,D) are the results from the two three-box layouts G3 and G3c, respectively; (E) shows the geometric mean of the deviation that have been calculated between the measurement position and the box representing the position, e.g., b_{FF} in the case of both FF3 and FF4 for the three-box layouts.

4. Discussion

4.1. Comparison with the Modelled Concentrations

In this study, we considered one-, two-, and three-box layouts in the chamber. On average, the concentrations for all of the geometrical layouts were estimated reliably within a factor of 0.5 and 2 of the measured concentrations, which has been used as a benchmark by Jayjock et al. [17]. The one-box layout underestimated the NF concentrations and overestimated the FF concentrations due to the direct dilution of the aerosols into a much larger volume than for any of the other geometries. The two-box model was found to provide the best overall fit for experiment E1 and E2 where the constantly active source caused stable concentrations and a reasonably fully mixed situation after the initial 900 s. In E1 the NF concentrations were underestimated by the two-box model by close to 25% due to high variation in the measured NF concentrations. This high variance might be due to the occurrence of eddy formation and cyclic directional transport in the NF due to a high AER in this experiment, meaning that a high concentration gradient and incomplete mixing in the NF could be expected.

Comparison of concentrations for the three-box layouts was made possible by having several measurement points in the chamber to record the differences in concentrations between NF, MF, and FF. The main differences between the two three-box layouts were the volumes of each box and the respective deposition areas. For G3c and G3, respectively, the b_{NF} and b_{MF} were 20% to 25% smaller, while b_{FF} was 47% larger. Despite this difference in volume division between the two layouts, they perform equally in predicting concentrations. For example, the difference in the modelled NF concentration between the two three-box layouts was negligible despite the NF volume was close to 25% smaller for G3c compared to G3 6.3 m³ and 8.3 m³, respectively. This would mean less dilution in the initial step in the NF for G3c, but the effect was negated by the transport and dilution into the MF. The inclusion of a MF limits flow to the FF in the model and improves the model quality, when mixing is limited by, e.g., cross flow by ventilation or walls. The three-box layouts better followed the timing of the peak concentrations and the broadening of the concentration peaks in MF and FF compared to the two-box and one-box layouts. Accurate timing is relevant if workers are present only during peak concentrations, but it is less critical if the concern is the overall average concentration.

Overall, a decreasing deviation from the measured concentration was observed with increasing complexity except for the position FF3, which displayed exceptional high concentrations when compared with, e.g., FF4 and FF2, and which was similarly underestimated in the models for all of the layouts. Since we assumed the chamber to be fully mixed at all times, the increased concentrations measured in the FF3 position were not replicated by the model, and thus the concentrations were underestimated in this position for all geometrical layouts. For comparison measurement and workplace measurements in general, the position of monitoring equipment is crucial as concentrations that were measured in FF4 were much different than in FF3 and would give a completely different concentration profile despite being close to the same distance from the source, 4.1 m and 4.7 m for FF3 and FF4, respectively.

4.2. Geometrical Layouts

Choosing a representative geometrical layout when approximating concentrations using multi-box models is a critical point. By splitting the chamber into multiple boxes, it is possible to increase the granularity, and thereby, achieving a better fit with the measured concentrations. But, as more boxes are added, more unknowns and parameters, such as flow between boxes and the geometrical parameterisation, which in turn, is linked to deposition parameters and influence on the exhaust removal via the general ventilation. The added parameters being introduced need to be fitted, this consequently increases the uncertainty in the model and makes it harder to apply the results to systems without reference concentrations. In this study, for the constant source in E1 and E2, no further significant increase in accuracy was found when increasing the geometrical complexity from a two-

to a three-box layout. Whereas, for the fluctuating source and low AER in E3, the timing of the peak concentrations were better estimated by the three-box layout.

The dispersion of aerosols is heavily dependent on the ventilation and air-flow, as this is conceptually the only method of mixing the aerosols inside the chamber besides convection-driven transport. This means that it is difficult to estimate the concentrations accurately by using multi-box models in an environment where the air is not well-mixed. For work in small chambers, a one- or two-box layout might be sufficient for accurate modelling depending on the mixing. For studies of workplaces and industrial facilities, the rooms are often comprised of large factory halls. In these facilities, the effect of the general ventilation on the flow between NF and FF is often limited, meaning long transport times and that natural convection plays an important role as well. Therefore, the assumption of fully mixed compartments might no longer be valid and directional transport similar as for the FF3 position in E2 and E3 will occur. The utility of the multi-box layouts should be tested in further experimental and field studies, ideally increasing the number of monitoring positions. In general, in the decision tree for choosing appropriate geometry for any modelling, the following should be taken into account: first, structures limiting the airflow and the transport of particles in the chamber; second, to determine location and use of the general and local ventilation; third, in the case of workers in the location, to take into account where they are located and to determine the relevant need for assessing their exposure, including any limitations with regards to the experimental setup. Other approaches to determine possible geometrical layouts include using Kriging methods on measured concentrations to fit the geometrical parameters or use computational fluid dynamics to calibrate the transport in the model and to design a multi-box layout based on the determined flow fields taking care of identifying potential dead zones in the chamber.

4.3. Measurements

In E1 and E2, the maximum concentrations were higher than in E3 due to the continuous source. The high AER meant a faster removal of particles from the FF, thus greater difference in between NF and FF concentrations than for low AER in the steady state experiments. In addition, the concentrations measured in the different FF positions were similar in magnitude during the steady state, with highest concentrations being measured in FF3. In this case, the chamber was assumed to be fully mixed after the first 900 s. The slower mixing in E3 caused the dilution of the dispersed aerosol to be slower, and, unlike in E1 and E2, coupled with short source active time of 2 min every 15 min, there was no steady state concentrations that were observed in E3. In general, for E3, there was a delay of 150 s before the concentration reached its maximum in the NF and further 175–450 s to increase to the maximum concentrations in the FF. The dilution caused the concentration peak to appear sharp closer to the source and broaden further from the source. Exception to this was the FF3 measurement position, which was closer in concentration magnitude to the NF concentration in both E2 and E3. These higher concentrations were not observed at FF4 even though FF3 and FF4 were of a similar distance from the source, while FF3 was closer to the exhaust with a distance of 1 m and 1.9 m for FF3 and FF4, respectively. However, since there was only one CPC that was located in the FF3 position, it was not possible to determine whether this was caused by an anomaly of the instrument or that the flow of particles by the air-flow from the ventilation caused a directional transport of the particles in both experiments, which would mean non-homogenous mixing in the chamber at low AER.

4.4. Outlook

Using models for workplace assessments by safety engineers in the industry requires a model that is fast and intuitive to use while providing reasonably accurate estimates of concentrations. The model computational time in the presented work was less than 30 s on a standard desktop computer. Adding a graphical user interface could make the use of the model an intuitive and easy experience for the safety engineer. Additionally, having a scenario library, as described in Koivisto et al. [5], or being compiled in the nano exposure & contextual information database [40], which includes the measured

source strengths and sample processes, would be a valuable inclusion as well. This would further tie in well with the current EU project caLIBRAte [41] intentions to systematise and homogenise the way data are collected and handled for the use in models. This allows for the use of modelling of real indoor working environments and a comparison of measured and modelled concentrations, while considering the decision tree for when to apply the use of multiple boxes in the geometrical layout of the model. While the present study has shown, especially the two- and three-box layouts predicted well the concentration levels in a well-controlled environment, the next step is to test the model performance by comparing modelled exposure levels with measured exposure levels in different environments. A successful comparison requires exposure studies, where contextual information is described well, and that concentrations are measured from multiple locations (see, e.g., occupational exposure studies by Jensen et al. [29], Koponen et al. [42], Mølgaard et al. [22], Koivisto et al. [25,43–45], and Fonseca et al. [46,47]). In addition, chamber studies will be carried out to characterise the significance of source strength measurements and the dispersion factor.

5. Conclusions

In the presented work, we have introduced a working multi-box aerosol model that is based on established aerosol physics and conceptual flow parameters. The particle population balance equation of the model includes a source generation, ventilation and transport, coagulation, and a deposition term. We used measured data from chamber experiments to compare with modelled concentrations. The experiments consisted of two different source generation schemes. In one case, the source was constant over 50 min with a high AER and more than 150 min with a low AER. In the third case, the source was a series of seven pulses of two minutes with a low AER. The chamber was monitored in six positions for accurate timing of concentration changes throughout the chamber.

With the model, we tested different geometrical layouts of the boxes in the model. A one-box, two-box, and two three-box layouts were used. The three-box layouts consisted of a square- and a cylindrical-shaped layout. We found that, for the constant source experiment, the two-box geometry provided the best overall fit at most of the locations with concentrations in all of the positions within $\pm 35\%$ of the measured concentrations, except in the case of position FF3 for low AER, while the one-box layout underestimated the concentrations in the NF and overestimated the concentrations in the FF. For the pulsating source, the three-box layout provided increased granularity and followed better the trends of the measured total number concentrations. The three-box layouts provided a better fit when compared with three out of five positions inside the chamber.

For a constant source and fast or slow mixing, the two-box model will provide an accurate estimation of the concentration, but chambers with a slow mixing rate, which means longer transport and mixing times, a multi-box approach, should be considered for providing more detailed granularity of the concentrations and a more accurate estimate of concentrations originating from a rapidly changing source.

Supplementary Materials: The following are available online at <http://www.mdpi.com/2076-3298/5/5/52/s1>.

Author Contributions: Miikka Dal Maso, Antti J. Koivisto, Emmanuel Belut, Asmus Meyer-Plath, Martie Van Tongeren, Araceli Sánchez Jiménez, Ilse Tuinman, Maida Domat, Jørn Toftum, and Ismo K. Koponen conceived and designed the experiments; Alexander C. Ø. Jensen, Antti J. Koivisto, Emmanuel Belut, Asmus Meyer-Plath, Ilse Tuinman, Maida Domat, Jørn Toftum, and Ismo K. Koponen performed the experiments; Alexander C. Ø. Jensen and Miikka Dal Maso analysed the data and coded the model; Alexander C. Ø. Jensen drafted the manuscript. All authors have revised the manuscript critically and read and approved the final manuscript.

Funding: This research was funded by The Danish Centre for Nanosafety II and the EU NANoREG framework programme (FP7/2007–2013) under grant agreement number 310584.

Conflicts of Interest: The authors declare no conflict of interest. The founding sponsors had no role in the design of the study; in the collection, analyses, or interpretation of data; in the writing of the manuscript, and in the decision to publish the results.

References

1. Piccinno, F.; Gottschalk, F.; Seeger, S.; Nowack, B. Industrial production quantities and uses of ten engineered nanomaterials in Europe and the world. *J. Nanopart. Res.* **2012**, *14*, 1109. [[CrossRef](#)]
2. Forster, S.; Olveria, S.; Seeger, S. Nanotechnology in the market: Promises and realities. *Int. J. Nanotechnol.* **2011**, *8*, 592–613. [[CrossRef](#)]
3. Hendren, C.; Mesnard, X.; Droge, J.; Wiesner, M. Estimating production data for five engineered nanomaterials as a basis for exposure assessment. *Environ. Sci. Technol.* **2011**, *45*, 2562–2569. [[CrossRef](#)] [[PubMed](#)]
4. Hansen, S.F.; Heggelund, L.R.; Besora, P.R.; Mackevica, A.; Boldrin, A.; Baun, A. Nanoproducts—What is actually available to European consumers? *Environ. Sci. Nano* **2016**, *3*, 169–180. [[CrossRef](#)]
5. Koivisto, A.J.; Jensen, A.C.Ø.; Kling, K.I.; Nørgaard, A.; Brinch, A.; Christensen, F.; Jensen, K.A. Quantitative material releases from products and articles containing manufactured nanomaterials: Towards a release library. *NanoImpact* **2017**, *5*, 119–132. [[CrossRef](#)]
6. Schulte, P.A.; Geraci, C.L.; Murashov, V.; Kuempel, E.D.; Zumwalde, R.D.; Castranova, V.; Hoover, M.D.; Hodson, L.; Martinez, K.F. Occupational safety and health criteria for responsible development of nanotechnology. *J. Nanopart. Res.* **2014**, *16*, 2153. [[CrossRef](#)] [[PubMed](#)]
7. Roldin, P.; Liao, L.; Mogensen, D.; Dal Maso, M.; Rusanen, A.; Kerminen, V.-M.; Mentel, T.F.; Wildt, J.; Kleist, E.; Kiendler-Scharr, A.; et al. Modelling the contribution of biogenic volatile organic compounds to new particle formation in the Jülich plant atmosphere chamber. *Atmos. Chem. Phys.* **2015**, *15*, 10777–10798. [[CrossRef](#)]
8. Johnson, M.; Lam, N.; Brant, S.; Gray, C.; Pennise, D. Modeling indoor air pollution from cookstove emissions in developing countries using a Monte Carlo single-box model. *Atmos. Environ.* **2011**, *45*, 3237–3243. [[CrossRef](#)]
9. Zhang, Y.; Banerjee, S.; Yang, R.; Lungu, C.; Ramachandran, G. Bayesian modeling of exposure and airflow using two-zone models. *Ann. Occup. Hyg.* **2009**, *53*, 409–424. [[CrossRef](#)] [[PubMed](#)]
10. Nazaroff, W.W.; Cass, G.R. Mathematical modeling of indoor aerosol dynamics. *Environ. Sci. Technol.* **1989**, *23*, 157–166. [[CrossRef](#)]
11. Li, X.; Niu, J.; Gao, N. Spatial distribution of human respiratory droplet residuals and exposure risk for the co-occupant under different ventilation methods. *HVAC&R Res.* **2011**, *17*, 432–445. [[CrossRef](#)]
12. Cheng, Y.S. Condensation detection and diffusion size separation techniques. In *Aerosol Measurements: Principles, Techniques and Applications*; Baron, P.A., Willeke, K., Eds.; Wiley-Interscience: New York, NY, USA, 2001; pp. 569–601.
13. Drivas, P.J.; Valberg, P.A.; Murphy, B.L.; Wilson, R. Modeling indoor air exposure from short-term point source releases. *Indoor Air* **1996**, *6*, 271–277. [[CrossRef](#)]
14. Chao, C.Y.H.; Wan, M.P. A study of the dispersion of expiratory aerosols in unidirectional downward and ceiling-return type airflows using a multiphase approach. *Indoor Air* **2006**, *16*, 296–312. [[CrossRef](#)] [[PubMed](#)]
15. Gao, N.; Niu, J. Modeling particle dispersion and deposition in indoor environments. *Atmos. Environ.* **2007**, *41*, 3862–3876. [[CrossRef](#)]
16. Chen, C.; Liu, W.; Lin, C.-H.; Chen, Q. Comparing the Markov chain model with the Eulerian and Lagrangian models for indoor transient particle transport simulations. *Aerosol Sci. Technol.* **2015**, *49*, 857–871. [[CrossRef](#)]
17. Jayjock, M.A.; Armstrong, T.; Taylor, M. The Daubert standard as applied to exposure assessment modeling using the two-zone (NF/FF) model estimation of indoor air breathing zone concentration as an example. *J. Occup. Environ. Hyg.* **2011**, *8*, D114–D122. [[CrossRef](#)] [[PubMed](#)]
18. Furtaw, E.J.; Pandian, M.D.; Nelson, D.R.; Behar, J.V. Modeling indoor air concentrations near emission sources in imperfectly mixed rooms. *J. Air Waste Manag. Assoc.* **1996**, *46*, 861–868. [[CrossRef](#)] [[PubMed](#)]
19. Nicas, M. Estimating exposure intensity in an imperfectly mixed room. *Am. Ind. Hyg. Assoc. J.* **1996**, *57*, 542–550. [[CrossRef](#)] [[PubMed](#)]
20. Cherrie, J.W.; Schneider, T. Validation of a new method for structured subjective assessment of past concentrations. *Ann. Occup. Hyg.* **1999**, *43*, 235–245. [[CrossRef](#)]
21. Hussein, T.; Korhonen, H.; Herrmann, E.; Hämeri, K.; Lehtinen, K.E.J.; Kulmala, M. Emission rates due to indoor activities: Indoor aerosol model development, evaluation, and applications. *Aerosol Sci. Technol.* **2005**, *39*, 1111–1127. [[CrossRef](#)]

22. Mølgaard, B.; Viitanen, A.K.; Kangas, A.; Huhtiniemi, M.; Larsen, S.T.; Vanhala, E.; Hussein, T.; Boor, B.E.; Hämeri, K.; Koivisto, A.J. Exposure to airborne particles and volatile organic compounds from polyurethane molding, spray painting. *Int. J. Environ. Res. Public Health* **2015**, *12*, 3756–3773. [[CrossRef](#)] [[PubMed](#)]
23. Cherrie, J.W.; MacCalman, L.; Fransman, W.; Tielemans, E.; Tischler, M.; Van Tongeren, M. Revisiting the effect of room size and general ventilation on the relationship between near- and far-field air concentrations. *Ann. Occup. Hyg.* **2011**, *55*, 1006–1015. [[CrossRef](#)] [[PubMed](#)]
24. Ganser, G.H.; Hewett, P. Models for nearly every occasion: Part II—Two box models. *J. Occup. Environ. Hyg.* **2017**, *14*, 58–71. [[CrossRef](#)] [[PubMed](#)]
25. Koivisto, A.J.; Jensen, A.C.Ø.; Levin, M.; Kling, K.I.; Dal Maso, M.; Nielsen, S.H.; Jensen, K.A.; Koponen, I.K. Testing the near field/far field model performance for prediction of particulate matter emissions in a paint factory. *Environ. Sci. Processes Impacts* **2015**, *17*, 62–73. [[CrossRef](#)] [[PubMed](#)]
26. *ECETOC Targeted Risk Assessment*; Technical Report No. 93; European Centre for Ecotoxicology and Toxicology of Chemicals: Brussels, Belgium, 2004.
27. Marquart, H.; Heussen, H.; Le Feber, M.; Noy, D.; Tielemans, E.; Schinkel, J.; West, J.; Van Der Schaaf, D. ‘Stoffenmanager’, a web-based control banding tool using an exposure process model. *Ann. Occup. Hyg.* **2008**, *52*, 429–441. [[CrossRef](#)] [[PubMed](#)]
28. Fransman, W.; Cherrie, J.; van Tongeren, M.; Schneider, T.; Tischler, M.; Schinkel, J.; Kromhout, H.; Warren, N.; Goede, H.; Tielemans, E. Advanced Reach Tool (ART): Development of the Mechanistic Model. *Ann. Occup. Hyg.* **2011**, *55*, 957–979. [[CrossRef](#)] [[PubMed](#)]
29. Jensen, A.C.Ø.; Levin, M.; Koivisto, A.J.; Kling, K.I.; Saber, A.T.; Koponen, I.K. Exposure assessment of particulate matter from abrasive treatment of carbon and glass fibre-reinforced epoxy-composites—Two case studies. *Aerosol. Air Qual. Res.* **2015**, *15*, 1906–1916. [[CrossRef](#)]
30. Seinfeld, J.H.; Pandis, S.N. *Atmospheric Chemistry and Physics: From Air Pollution to Climate Change*, 3rd ed.; John Wiley & Sons: Hoboken, NJ, USA, 2016.
31. Jacobson, M.Z. *Fundamentals of Atmospheric Modeling*, 2nd ed.; Cambridge University Press: Cambridge, UK, 2005.
32. Fuchs, N.A. *The Mechanics of Aerosols*; Pergamon Press: Oxford, UK; The Macmillan Company: New York, NY, USA, 1964.
33. Lai, A.C.K.; Nazaroff, W.W. Modeling indoor particle deposition from turbulent flow onto smooth surfaces. *J. Aerosol Sci.* **2000**, *31*, 463–476. [[CrossRef](#)]
34. Shi, S.; Zhao, B. Deposition of Indoor Airborne Particles onto Human Body Surfaces: A Modeling Analysis and Manikin-Based Experimental Study. *Aerosol Sci. Technol.* **2013**, *47*, 1363–1373. [[CrossRef](#)]
35. Shampine, L.F.; Reichelt, M.W. The MATLAB ODE Suite. *SIAM J. Sci. Comput.* **1997**, *18*, 1–22. [[CrossRef](#)]
36. Dormand, J.R.; Prince, P.J. A family of embedded Runge-Kutta formulae. *J. Comput. Appl. Math.* **1980**, *6*, 19–26. [[CrossRef](#)]
37. Saltelli, A.; Ratto, M.; Andres, T.; Campolongo, F.; Cariboni, J.; Gatelli, D.; Gatelli, D.; Saisana, M.; Tarantola, S. *Global Sensitivity Analysis. The Primer*; John Wiley & Sons Ltd.: West Sussex, UK, 2008.
38. Meyer-Plath, A.; Koponen, I.K.; Jensen, A.C.Ø.; Koivisto, A.J.; Belut, E.; Sánchez, A.; van Tongeren, M.; MacCalman, L.; Tuinman, I.; Fransman, W.; et al. NANoREG Report D3.4. Available online: http://www.rivm.nl/en/About_RIVM/International_Affairs/International_Projects/Completed/NANoREG/deliverables/NANoREG_D3_04_DR_Improved_data_for_the_modelling_of_the_exposure_to_MNMs.pdf (accessed on 8 February 2018).
39. Levin, M.; Gudmundsson, A.; Pagels, J.H.; Fierz, M.; Møhlhave, K.; Löndahl, J.; Jensen, K.A.; Koponen, I.K. Limitations in the Use of Unipolar Charging for Electrical Mobility Sizing Instruments: A Study of the Fast Mobility Particle Sizer. *Aerosol Sci. Technol.* **2015**, *49*, 556–565. [[CrossRef](#)]
40. Pelzer, J.; Schumacher, C. Nano Exposure & Contextual Information Database. Available online: <http://www.perosh.eu/research-projects/perosh-projects/necid/> (accessed on 8 February 2018).
41. CaLIBRAte Project, EU Horizon 2020 Grant Agreement 686239. Available online: www.nanocalibrate.eu (accessed on 8 February 2018).
42. Koponen, I.K.; Koivisto, A.J.; Jensen, K.A. Worker Exposure and High Time-Resolution Analyses of Process-Related Submicrometre Particle Concentrations at Mixing Stations in Two Paint Factories. *Ann. Occup. Hyg.* **2015**, *59*, 749–763. [[CrossRef](#)] [[PubMed](#)]

43. Koivisto, A.J.; Palomäki, J.E.; Viitanen, A.-K.; Siivola, K.M.; Koponen, I.K.; Yu, M.; Kanerva, T.S.; Norppa, H.; Alenius, H.T.; Hussein, T.; et al. Range-Finding Risk Assessment of Inhalation Exposure to Nanodiamonds in a Laboratory Environment. *Int. J. Environ. Res. Public Health* **2014**, *11*, 5382–5402. [[CrossRef](#)] [[PubMed](#)]
44. Koivisto, A.J.; Brostrøm, A.; Kling, K.I.; Fonseca, A.S.; Redant, E.; Andrade, F.; Hougaard, K.S.; Krepker, M.; Prinz, O.S.; Segal, E.; et al. Occupational exposure during handling and loading of halloysite nanotubes—A case study of counting nanofibers. *Nanoimpact* **2018**, accepted. [[CrossRef](#)]
45. Koivisto, A.J.; Kling, K.I.; Fonseca, A.S.; Bluhme, A.B.; Moreman, M.; Yu, M.; Costa, A.L.; Giovanni, B.; Ortelli, S.; Fransman, W. Dip coating of air purifier ceramic honeycombs with photocatalytic TiO₂ nanoparticles: A case study for occupational exposure. *Sci. Total Environ.* **2018**, *630*, 1283–1291. [[CrossRef](#)] [[PubMed](#)]
46. Fonseca, A.S.; Viitanen, A.-K.; Koivisto, A.J.; Kangas, A.; Huhtiniemi, M.; Hussein, T.; Vanhala, E.; Viana, M.; Querol, X.; Hämeri, K. Characterization of exposure to carbon nanotubes in an industrial setting. *Ann. Occup. Hyg.* **2015**, *59*, 586–599. [[CrossRef](#)] [[PubMed](#)]
47. Fonseca, A.S.; Kuijpers, E.; Kling, K.I.; Levin, M.; Koivisto, A.J.; Nielsen, S.H.; Fransman, W.; Fedutik, Y.; Jensen, K.A.; Koponen, I.K. Particle release and control of worker exposure during laboratory-scale synthesis, handling and simulated spills of manufactured nanomaterials in fume-hoods. *J. Nanopart. Res.* **2018**, *20*, 48. [[CrossRef](#)] [[PubMed](#)]



© 2018 by the authors. Licensee MDPI, Basel, Switzerland. This article is an open access article distributed under the terms and conditions of the Creative Commons Attribution (CC BY) license (<http://creativecommons.org/licenses/by/4.0/>).